Supplementary material

S1. Evaluation of workflow performance

A general goal of any data collection workflow is to maximize the amount of time the scanner is collecting useful data relative to time spent transporting it between stations, measuring target locations, or waiting for some other task to finish. In our TLS field surveys we find that the scan rate (data collection speed of the scanner) tends to be the most common time-limiting step, though with the higher scan rates of newer instruments, target acquisition can be equally time limiting. The following sections discuss factors in the data collection method presented here that we find influence scan efficiency, based on our DVF surveys and additional scanning experiences.

S.1.1 Site selection and survey planning

Mitigating the impact of local topography and vegetation on scan efficiency requires careful evaluation of potential field areas, assiduous site selection, and survey planning. Local topographic relief can either expedite the survey if it provides vantage points from which to conduct large overview scans, or increase scan time if it produces data shadows that require additional scan stations to infill. Vegetation in the scanned area will always result in data shadows. Uneven point spacing primarily results from data shadowing produced by vegetation or topography. Data shadowing is amplified on gently sloping surfaces that lie at a low angle to the scanner look direction, such as alluvial fans. Because field sites are generally unique, no single workflow can address problems with

data shadowing, thus strategies for minimizing data shadows must be developed or modified on a site-by-site basis. Considering the scientific value of a site and the practicality of scanning it are equally important because even dense scanning of a highly vegetated or topographically complex site may not yield the information needed to sufficiently characterize the features of interest. Likewise, choosing a site that is too big to scan in a reasonable period of time can result in aborted scans and wasted time.

Planning the scan sequence ahead of data collection can increase scan efficiency by minimizing the number of scan stations, each of which costs ~30 minutes to transport and set up the equipment, scan targets, and define the scan area. In planning the scan and installing ground control, we focus less on identifying scan locations than we do on choosing optimal target locations, i.e., those positions that ensure a maximum number of targets can be measured from anywhere within the field area. Actual scanner locations are somewhat flexible because we locate the scanner in the ground control network via target scans but do not set it up over a ground control point, so that final scanner positions can be adjusted in response to where data is needed.

S.1.2 Examples of site-morphology effects

The sites in this study were relatively small, so scan efficiency was dominantly controlled by the local site relief rather than other workflow steps. The effect of relief on scan efficiency is demonstrated by the number of stations and scan time, with Site 3 requiring over twice as many scanner locations as Site 6 (14 vs. 6) and almost three times as long (27 hrs vs. 10 hrs), even though both sites are approximately equal in area (4000 m^2 vs 3700 m^2) and Site 6 had over twice the point density of Site 3. The difference does not result from variations in external vantage points or vegetation, because neither site

had a good vantage point for an overview scan, and vegetation was similar at both (Fig. 6). Rather, the difference lies in the local slope and topographic relief: Site 3 lies on a gently (11°) sloping alluvial fan surface cut by a ~2 m deep channel and ~3 m deep graben, whereas at Site 6 the surface slopes more steeply (16°) and the channel and graben are both shallower (~0.4 m and ~2 m, respectively). At Site 3, the shallow slope and deep features combined to amplify shadowing, which required more scan stations and more time to fill in.

S.1.3 Target-based registration and scan flexibility

Using targets to register point clouds and the total station to measure the ground control network adds survey equipment and reduces mobility. However, a primary advantage of target-based methods is that each new scan is registered in the project as it is collected so that data completeness can be assessed continually while still in the field. Experience has shown that performing field registration by placing the data in an external reference frame is often less problematic than attempting to register scans in a scanner-centric reference frame defined only by target measurements, especially if targets have been repositioned during the survey.

Point-based feature matching is an alternative method for registering scans, but is not efficiently completed in the field. The key distinction between target- and feature-based registration methods is that in target-based methods, registration is accomplished by matching target center-point coordinates calculated from scans of targets of known dimension, whereas in feature-based methods, registration is accomplished by matching two overlapping point clouds. The advantage of target-based methods is that targets can be rotated to face the scanner while maintaining constant center position so that the

scanner has the same view of a target no matter where the scanner is placed. This means that each center point calculation for a particular target is calculated from a scan that is essentially the same in all but orientation to those collected for that target from all other scanner stations. In contrast, feature-based registration is complicated by the fact that while points collected by the scanner at different locations overlap and measure the same feature, they do not measure the same part of the feature because unlike targets, it is not being rotated to give the scanner an equal view from all scanner positions. This means that registration is accomplished by matching datasets that are similar, but necessarily different. Due to the uncertainty inherent in the feature-based registration process (which we have not attempted to quantify), and the fact that this process is not efficiently completed while still in the field, we consider target-based registration to be a more robust method for registering multiple point clouds into a composite dataset.

Target registration can be accomplished using several different common types of targets. These include prisms, spheres, cylinders, and planar reflective panels, the latter being the target type we use in this study. In contrast to panel targets, sphere and cylinder targets require no rotation to face the scanner and their center is calculated automatically for a given diameter. We have little experience with registration using anything but panel targets, however, because the quality of a laser return is greatly decreased with increased obliquity of the measured surface to the laser beam, the center of a panel target will be calculated from a denser population of high quality measurements because its entire face is essentially orthogonal to the laser beam, whereas strictly speaking, measurements of equal quality will be collected at only one point on a sphere, and along only one line on a cylinder, with the rest decreasing in quality as the surface of the cylinder or sphere curves

away from the scanner. This means that everything else being equal, the average quality of data used to calculate the center of a sphere or cylinder is less than that used to calculate the center of a panel target.

Independent measurements of the ground control network increase efficiency and flexibility during data collection. In purely target-based methods (i.e. no ground control network is installed) a minimum of two targets common between scans is required to place a leveled scanner within the previously scanned target network and to accurately register point clouds. In some situations this requirement can be difficult to meet without moving targets that may be needed in future scans. The independent network allows scans from two stations to be accurately co-registered even if no common targets are scanned between the two stations. Importantly, the network also allows scans to be registered using targets that are at different elevations over the same control point in case targets need to be repositioned between scans. This is a key advantage when scanning with a limited number of target assemblies (e.g., 2), in which case more frequent repositioning is required to scan enough targets from each station, or if targets must be taken down overnight or re-adjusted in response to environmental changes (e.g., wind, rain, ungulates). Removing the need to scan common targets and having the ability to reposition targets to serve a scanner position means that scanner positions can be chosen where they will maximize coverage of key features, rather than on the basis of which or how many targets can be measured. In the case where problems are discovered with the automatic target registration after leaving the field, experience has shown that having independently constrained measurements of target positions can allow the scans to be registered using point based registration of the target centers.

S.1.4 Single-surveyor scanning

Installing and measuring the ground control network, setting up and measuring targets, and transporting equipment between scanner stations constitute additional steps in the scanning workflow that take time. In many cases, the reduction in efficiency imposed by these steps can be minimized by conducting operations in parallel (e.g., measuring ground control while the scanner is running), and by minimizing the need to reposition targets by placing them so they are visible from numerous locations throughout the field area. The scanner, a tripod, generator, and laptop are all that is required at each scan station, and can be moved by a single person in one trip.

However, single-user operation breaks down under several circumstances. One is where sites are large or topographically complex, so that targets need to be repositioned frequently. This problem is made worse when using fewer target assemblies. Large and complex sites also take longer to traverse, reducing the speed with which a single user can collect ground control measurements or move equipment between scan stations. Likewise an increase in the number of trips needed to move equipment, such as when batteries are used for power, can inhibit single user operation. In addition, data collection speeds (pts/second) of newer instruments have increased to the point where data collection no longer consumes enough time to complete tasks in parallel so that surveys can be more efficiently collected with two workers, where one scans and the other installs or re-orients targets as needed.

S2. Method for manual slip vector measurements

The following description expands upon that given in Section 3.4. Let the intersection of the fault with the feature in the footwall and hanging wall be the points $x_1y_1z_1$, and $x_2y_2z_2$, respectively. In a footwall-fixed reference frame, the slip vector **v** is then

$$\mathbf{v} = L\boldsymbol{i} + M\boldsymbol{j} + N\boldsymbol{k}, \quad (1)$$

where

$$L = (x_2 - x_1)$$

$$M = (y_2 - y_1)$$

$$N = (z_2 - z_1).$$

The trend (T) and plunge (P) of the slip vector **v** are then given by

$$T = \text{atan}\left(\frac{M}{L}\right), \quad (2)$$

$$P = \text{atan}\left(\frac{N}{\sqrt{L^2 + M^2}}\right), \quad (3)$$

and the magnitude of the displacement is given by

$$D = \text{sqrt}\,(L^2 + M^2 + N^2). \quad (4)$$

In the case of conjugate faults, it is necessary to calculate a slip vector for displacement on both faults and then sum these vectors to obtain the total slip vector, as shown in Figure 3C. In this case we define the slip vectors in the synthetic and antithetic fault planes as $\mathbf{v_1}$ and $\mathbf{v_2}$, respectively, where,

$$\mathbf{v_1} = L_1\boldsymbol{i} + M_1\boldsymbol{j} + N_1\boldsymbol{k}, \quad (5)$$

$$\mathbf{v_2} = L_2\boldsymbol{i} + M_2\boldsymbol{j} + N_2\boldsymbol{k}, \quad (6)$$

with

$$L_1 = (x_2 - x_1)$$

$$M_1 = (y_2 - y_1)$$

$$N_1 = (z_2 - z_1)$$

and

$$L_2 = (x_4 - x_3)$$

$$M_2 = (y_4 - y_3)$$

$$N_2 = (z_4 - z_3).$$

The total slip vector $\mathbf{v}_T$ is then determined by

$$\mathbf{v}_T = \mathbf{v_1} + \mathbf{v_2} = L_T\boldsymbol{i} + M_T\boldsymbol{j} + N_T\boldsymbol{k}, \quad (7)$$

where

$$L_T = (x_2 - x_1) + (x_4 - x_3)$$

$$M_T = (y_2 - y_1) + (y_4 - y_3)$$

$$N_T = (z_2 - z_1) + (z_4 - z_3).$$

The trend (T_T) and plunge (P_T) of the total slip vector are determined by substituting L_T, M_T, and N_T in Equations 2 and 3. This slip vector will not lie in either of the fault planes defined at the surface, rather it lies in the fault plane at depth. The dip of the fault at depth (d) can then be determined by computing the plane containing the total slip vector and the line of fault strike

$$d = \text{atan}\left(\frac{\tan(P_T)}{\sin(Q)}\right), \quad (8)$$

where Q is the angle between regional fault strike (S) and the trend of the total slip vector (T_T) and is determined by

$$Q = S + T_T. \quad (9)$$

S3. Method for automated iterative slip vector measurements

The following description and Figure S1 compliment Section 3.5.

I. Geometric primitive inputs (measured using LidarViewer):

A. Fan surfaces *1* and *5*

B. Graben surface *3*

C. Fault planes *2* and *4*

D. Offset linear feature lines *L1* and *L2*

II. Calculate dip slip magnitude (component of slip orthogonal to graben)

A. Calculate 3D orientations of intersection lines *1-4* between fan, fault and graben planes

B. Calculate intersection points Lp_1 and Lp_2 (black circles, Fig. S1) between linear features *L1* and *L2* and the adjacent faults *2* and *4*, respectively.

C. Calculate a cross section plane (cp) oriented orthogonally to the average orientation of intersection lines *1-4* and centered between the line-fault intersection points Cp_1-Cp_4. The vertical and extensional components of the slip vector that define the graben-orthogonal component of slip lie in the *cp* plane. All quantities calculated in the following steps d-h are 2D and lie within this plane.

D. Calculate intersections between plane intersection lines *1-4* and the cross section plane (red circles).

E. Calculate the width of the graben as:

i. $g_w = ||Cp_3 - Cp_2||$.

F. Calculate orientation (normal vector and direction) of graben line (g) within the cross section plane.

1. The normal vector (g_n) is defined as bisecting the orientations of the normal vectors to fan surface lines *1* and *5*.
2. The direction (g_d) is:
    i. $g_d = g_n \times cp$ (make unit length).

G. Calculate fault-orthogonal displacement (lies in cross-section plane *cp*):

i. $v_d = Cp_4 - (Cp_1 + g_d \cdot g_w)$.

H. And calculate the reconstructed position of LP_2 as:

i. $LP_2' = Lp_2 - v_d$.

III. Calculate lateral slip magnitude (component of slip parallel to fault planes)

A. In map view, project linear feature lines *L1* and *L2'* vertically to parallelism with fan planes *1* and *5'*, respectively.

B. Project lines *L1* and *L2'* across the graben to fault planes on opposite side, and calculate intersection point Lp_1P and $Lp_2'P$.

C. Calculate fault parallel slip $V||_1$ and $V||_2$:

i. $V||_1 = Lp_1 - Lp_2'P$

ii. $V||_2 = Lp_1P - Lp_2'$.

D. Calculate the final displacement vector:

i. $V = v_d + V||_1 \cdot (\lambda) + V||_2 \cdot (1-\lambda)$, where $\lambda \in [0,1]$.

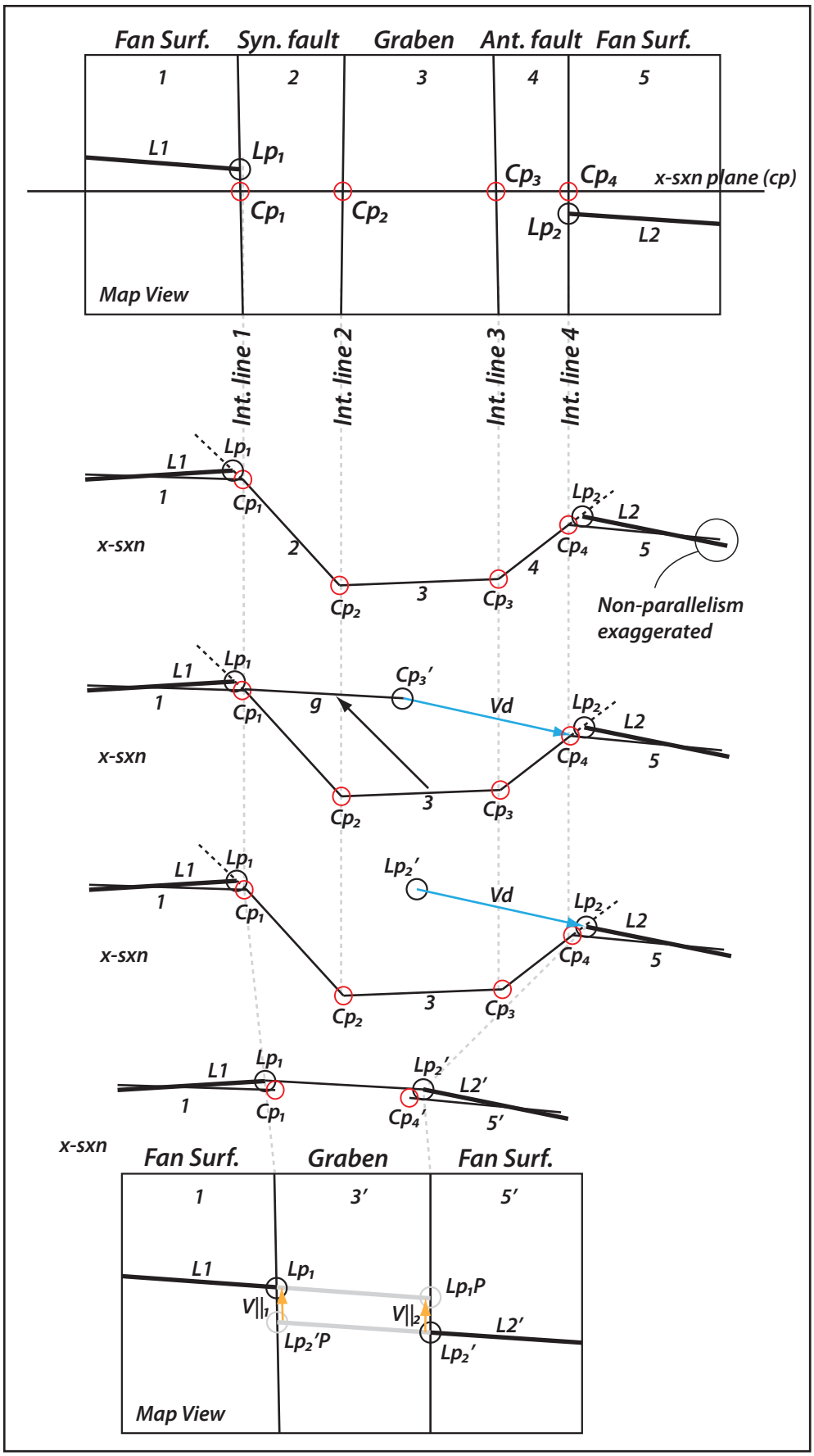
Fan Surf.
Syn. fault
Graben
Ant. fault
Fan Surf.
1
2
3
4
5
L1
Lp1
Cp3
Cp4
x-sxn plane (cp)
Cp1
Cp2
Lp2
L2
Map View
Int. line 1
Int. line 2
Int. line 3
Int. line 4
x-sxn
Non-parallelism exaggerated
g
Vd
Lp2′
Cp3′
L2′
5′
Fan Surf.
Graben
Fan Surf.
3′
Lp1P
V||1
V||2
Lp2′P
Map View

Figure S1

TABLE S1: INSTRUMENT SPECIFICATIONS[1]

Instrument	Make/Model	Max Range	Accuracy	Precision		
				Distance	Horizontal	Vertical
Total Station	Leica TCR 407 Power	3500 m	2 mm @ 100 m	.2 mm @ 100 m	3.4 mm	3.4 mm
Laser Scanner	Trimble GX DR 200+[2,3]	350 m	7 mm @ 100 m	2.5 mm @ 100 m	5.8 mm	6.8 mm
		Processor		**Memory**	**Graphics**	
Ruggedized Laptop	Dell Latitude ATG D620	2.33 GHz Intel Core 2 Duo		2 GB RAM	Intel GMA 950	

[1]The stated values are those reported by the manufacturer and assume ideally reflective surfaces with no obliquity to the infrared or laser light beams; we have not independently assessed these specific accuracy and precision measurements under realistic field conditions.

[2]3.2 mm minimum point spacing at 100 m

[3]3 mm diameter laser spot size at 50 m

TABLE S2: COMPARISON OF TARGET-TO-TARGET DISTANCES				
Measured Distances (m)				
Target Pair	**Method 1[1]**	**Method 2[2]**	**Method 3[3]**	**Method 4[4]**
1-2	109.409	109.411	109.409	109.420
2-3	24.558	24.568	24.564	24.567
3-4	109.036	109.046	109.040	109.049
4-1	28.533	28.539	28.533	28.528
2-4	111.910	111.918	111.912	111.920
1-3	112.857	112.865	112.861	112.871
Distance Differences relative to Method 3 (m)				
Target Pair	**Method 1**	**Method 2**	**Method 3**	**Method 4**
1-2	0.000	0.002	–	0.011
2-3	0.006	0.004	–	0.003
3-4	0.005	0.006	–	0.008
4-1	0.001	0.006	–	0.005
2-4	0.002	0.006	–	0.009
1-3	0.004	0.004	–	0.010

[1]Total station, prism on survey pole

[2]Total station, prism on tripod

[3]Total station, target on tripod

[4]Laser scanner, target on tripod

TABLE S3: SCAN REGISTRATION EXPERIMENT RESULTS

Simulated Workflow	Scan Station	Apex Coordinates (m)			Pyramid Offset (m)				Residual Target Error (m)	
		x	y	z	Δx	Δy	Δz	total[1]	By Station	Average
Method 1:Total Station, Prism on Survey Pole										
1	1	0.1031	-33.0078	-0.5994	0.0040	0.0018	0.0002	0.0044	0.0108	0.0091
	2	0.0992	-33.0060	-0.5996					0.0074	
2	1	0.1049	-33.0107	-0.6001	0.0041	0.0026	0.0002	0.0048	0.0111	0.0090
	2	0.1008	-33.0081	-0.6003					0.0069	
3	1	0.0988	-33.0105	-0.6002	0.0002	0.0043	0.0010	0.0044	0.0062	0.0063
	2	0.0986	-33.0062	-0.5992					0.0063	
4	1	0.1110	-33.0013	-0.5967	0.0124	0.0012	0.0001	0.0125	0.0030	0.0028
	2	0.0986	-33.0001	-0.5966					0.0026	
5	1	0.1053	-33.0139	-0.6021	0.0009	0.0022	0.0005	0.0024	0.0123	0.0081
	2	0.1044	-33.0117	-0.6026					0.0039	
6	1	0.1106	-33.0089	-0.5980	0.0081	0.0024	0.0013	0.0085	0.0066	0.0070
	2	0.1025	-33.0065	-0.5993					0.0074	
7	1	0.0976	-33.0060	-0.5992	0.0002	0.0022	0.0008	0.0023	0.0078	0.0069
	2	0.0974	-33.0038	-0.5985					0.0061	
Method 2: Total Station, Prism on Tripod										
1	1	0.1046	-33.0090	-0.5966	0.0040	0.0019	0.0002	0.0044	0.0077	0.0066
	2	0.1005	-33.0071	-0.5968					0.0055	
2	1	0.1076	-33.0102	-0.5975	0.0040	0.0027	0.0002	0.0048	0.0067	0.0054
	2	0.1036	-33.0075	-0.5977					0.0041	
3	1	0.1040	-33.0115	-0.5972	0.0003	0.0044	0.0010	0.0045	0.0038	0.0041
	2	0.1038	-33.0071	-0.5962					0.0043	
4	1	0.1043	-33.0060	-0.5952	0.0123	0.0013	0.0001	0.0124	0.0060	0.0058
	2	0.0920	-33.0047	-0.5951					0.0056	
5	1	0.0976	-33.0123	-0.5981	0.0009	0.0022	0.0005	0.0024	0.0076	0.0049
	2	0.0967	-33.0101	-0.5986					0.0022	
6	1	0.0979	-33.0099	-0.5963	0.0002	0.0010	0.0009	0.0013	0.0044	0.0031
	2	0.0981	-33.0089	-0.5954					0.0017	
7	1	0.1011	-33.0088	-0.5962	0.0003	0.0022	0.0007	0.0023	0.0065	0.0061
	2	0.1008	-33.0066	-0.5955					0.0058	
Method 3: Total Station, Target on Tripod										
1	1	0.1026	-33.0095	-0.6001	0.0039	0.0019	0.0002	0.0043	0.0092	0.0079
	2	0.0987	-33.0076	-0.6003					0.0065	
2	1	0.1043	-33.0118	-0.6010	0.0041	0.0027	0.0003	0.0049	0.0094	0.0078
	2	0.1002	-33.0091	-0.6014					0.0061	
3	1	0.0995	-33.0123	-0.6002	0.0002	0.0044	0.0011	0.0045	0.0062	0.0063
	2	0.0993	-33.0079	-0.5991					0.0063	
4	1	0.1078	-33.0042	-0.5966	0.0123	0.0012	0.0001	0.0124	0.0030	0.0028
	2	0.0955	-33.0030	-0.5966					0.0027	
5	1	0.0980	-33.0147	-0.6036	0.0008	0.0021	0.0004	0.0023	0.0096	0.0059
	2	0.0972	-33.0126	-0.6041					0.0022	
6	1	0.1089	-33.0095	-0.5995	0.0082	0.0024	0.0013	0.0086	0.0057	0.0063
	2	0.1007	-33.0071	-0.6008					0.0068	
7	1	0.0983	-33.0085	-0.5992	0.0002	0.0023	0.0007	0.0024	0.0072	0.0065
	2	0.0980	-33.0062	-0.5985					0.0057	

TABLE S3 Continued: SCAN REGISTRATION EXPERIMENT RESULTS

Method 4: Laser Scanner, Target on Tripod										
Simulated	Scan	Apex Coordinates (m)			Pyramid Offset (m)				Residual Target Error (m)	
Workflow	Station	x	y	z	Δx	Δy	Δz	total	By Station	Average
1	1	-25.5425	20.1865	-0.2660	0.0043	0.0011	0.0002	0.0044	0.0027	0.0027
	2	-25.5468	20.1854	-0.2663					0.0027	
2	1	-25.5426	20.1864	-0.2660	0.0048	0.0005	0.0002	0.0048	0.0030	0.0030
	2	-25.5474	20.1859	-0.2663					0.0030	
3	1	-25.5425	20.1864	-0.2660	0.0029	0.0034	0.0011	0.0046	0.0005	0.0005
	2	-25.5454	20.1898	-0.2650					0.0005	
4	1	-25.5426	20.1864	-0.2661	0.0105	0.0065	0.0001	0.0123	0.0002	0.0002
	2	-25.5531	20.1799	-0.2660					0.0002	
5	1	-25.5426	20.1864	-0.2660	0.0020	0.0013	0.0005	0.0024	0.0042	0.0042
	2	-25.5446	20.1877	-0.2665					0.0042	
6	1	-25.5426	20.1864	-0.2661	0.0004	0.0010	0.0009	0.0014	0.0014	0.0014
	2	-25.5430	20.1874	-0.2652					0.0014	
7	1	-25.5425	20.1865	-0.2660	0.0017	0.0016	0.0006	0.0024	0.0014	0.0014
	2	-25.5442	20.1881	-0.2654					0.0014	

[1]~1.6 mm error determined from RMS fit of planes to points defining pyramid sides.